ADVANCED ENERGY MATERIALS
www.advenergymat.de

Electrochemical Supercapacitors: From Mechanism Understanding to Multifunctional Applications

*Jingwei Chen and Pooi See Lee**

Electrochemical supercapacitors (SC) with high power and long cycle life have been extensively studied and applied in certain areas. However, a majority of the efforts have been devoted to developing SCs with improved performance through novel electrode/electrolytes design. The full mechanistic understanding of SCs based on different electrode materials has not yet been realized. In addition, exploration of new functions for SCs to widen their applications must be accelerated. In this essay, the use of advanced characterization methods (in situ X-ray diffraction, in situ X-ray scattering, in situ atomic force microscopy, in situ nuclear magnetic resonance, in situ Raman/infrared spectroscopy, electrochemical quartz crystal microbalance, scanning electrochemical microscopy, etc.) to unveil the electrochemical process of SCs from different aspects will be discussed. The working principles, information to be extracted, and case studies of respective methods will be presented. The multipronged mechanism studies of electrode properties inspire and enable exploration of extra functions within the same electrochemical SCs. Realization of mechanically deformable, low-temperature, color tunable, self-healable, and self-chargeable SCs; integrated SC-sensors; and SC-actuators with adoption of new electrode/electrolyte/current collectors/configurations are showcased. The remaining issues hindering the wide exploitation of SCs and the future development trend of SCs are also discussed.

1. Introduction

Electrochemical supercapacitors (SC), with distinguished high power and superior cycling stability, have been a hotspot in academic research in the last two decades.[1–3] As complementary energy storage devices to batteries, electrochemical SCs are designated to find applications in consumer electronics, electric vehicles, and emergency power supplies, etc.[2] Variety of materials (carbon-based materials, metal oxides, conductive polymers, etc.) and multipronged approaches (surface area/pore structure control, heterostructure design, doping, crystal structure engineering, current collector modification, etc.) to assemble SCs with high performances have been explored.[1,2,4,5] Improved specific capacitance, rate performance, energy density, and cycling stability of SCs have been realized.[2,4]

During the charge–discharge process, complicated structural/physical/chemical properties variations of electrode materials are accompanied. Changes in lattice parameters, ion adsorption/desorption, chemical bonding formation/breakage, dimensional/mass change, etc., are involved in the electrochemical process.[6–9] Several advanced characterization techniques (in situ X-ray diffraction [XRD], in situ X-ray scattering, in situ atomic force microscopy [AFM], in situ nuclear magnetic resonance [NMR], in situ Raman/infrared (IR) spectroscopy, electrochemical quartz crystal microbalance [EQCM], scanning electrochemical microscopy [SECM], etc.) have been utilized to study the dynamic processes in SCs.[6,8,10–14] The information extracted varies for different characterization techniques, complementing each other to establish a more comprehensive mechanism understanding of SCs.

Electrochemical SCs are primarily energy storage devices, notably, new functionalities can be introduced into SCs through configuration modification or integration, catering the needs of efficient, flexible, and sustainable electronics.[2] With adoption of new electrodes/electrolytes/current collectors and different integration approaches, mechanically deformable SCs with flexibility or stretchability, self-healable SCs, low-temperature SCs, color tunable SCs, self-chargeable SCs, integrated SC-sensors, SC-actuators, etc., have been attempted and prototyped in the literature.[15–20]

Despite the success in design and assembly of high performance SCs, the electrochemical mechanisms of SCs based on different electrode materials are still not fully understood. In addition, the possibilities of novel functions incorporated

Dr. J. Chen, Prof. P. S. Lee
School of Materials Science and Engineering
Nanyang Technological University
Singapore 639798, Singapore
E-mail: pslee@ntu.edu.sg
Dr. J. Chen, Prof. P. S. Lee
Singapore-HUJ Alliance for Research and Enterprise (SHARE)
Nanomaterials for Energy and Energy Water Nexus (NEW)
Campus for Research Excellence and Technological Enterprise (CREATE)
Singapore 138602, Singapore
The ORCID identification number(s) for the author(s) of this article can be found under https://doi.org/10.1002/aenm.202003311.

DOI: 10.1002/aenm.202003311

into SCs are also not entirely explored. Multifaceted mechanism investigation of electrochemical SCs help to understand and refine the fundamental processes involved, while the exploration of new functionalities for electrochemical SCs can widen the possible application fields. In this essay, the advanced characterization techniques employed for electrochemical SC studies and the examples of multifunctional SCs will be summarized. The advanced (mostly in situ) characterization techniques will be classified into four sections based on the information derived, including changes in crystal structures, physical, chemical, or electrochemical properties variation. The principles of the respective methods will be briefly stated, followed by case studies to illustrate the findings derived. The attempts to fabricate mechanically deformable, low-temperature SCs, self-chargeable, and electrochromic (EC) SCs as well as SC-sensors, SC-actuators, etc., will be presented. This essay serves as a toolbox to researchers, displaying the available toolkits to gain a deeper understanding of SCs, as well as the possibilities to realize extra functions in SCs for more than merely energy storage applications.

2. Mechanism Understanding of Electrochemical Supercapacitors

During the electrochemical reactions, SC electrodes will undergo a series of physical/chemical/structural properties variations, including but not limited to crystal planes expansion/shrinkage, ion confinement/exchange in nanopores, geometry (thickness and lateral dimensions) variation, chemical bonding/oxidation state variations, etc.[6–9] These dynamic changes can be investigated with multiple techniques to provide more insights in the electrochemical mechanism of SCs. Considering the advantages of real time data acquisition of in situ/operando characterization versus ex situ methods,[21] more focus will be placed on in situ/operando methods in this section. The various methods will be classified into four sections based on the information to be extracted: crystal structure, physical properties, chemical properties, and electrochemical properties. Representative examples of advanced characterization methods to explore the electrochemical mechanisms of SCs have been summarized in **Figure 1**. The characterization methods reported in literature will be discussed, accompanied by brief introduction on the working principles and the information to be derived, followed by case studies.

2.1. Crystal Structures Variation

Electrode materials of electrochemical SCs are normally classified into two groups: i) non-Faradaic materials based on electrical double layer capacitance (mostly carbon materials); ii) Faradaic materials with pseudocapacitance (e.g., metal oxides, metal nitrides, metal carbides, etc.). The electrochemical process of the latter often involves ion intercalation/de-intercalation into the crystal structure, causing reversible lattice parameter variation during the charge storage.

2.1.1. In Situ X-Ray Diffraction

In situ XRD can reveal the crystal structure variation during electrochemical process, for pseudocapacitive materials including metal oxides and MXenes.[6,22,28,29] Multiple cations (Li^+, Na^+, K^+, Al^{3+}, NH_4^+, and Mg^{2+}) can be intercalated into Ti_3C_2 MXene layers in aqueous electrolyte, offering capacitance higher than 300 F cm^{-3}.[29] Shrinkage of MXene layers upon cathodic K^+ and Mg^{2+} intercalation was verified with in situ XRD characterization, possibly due to the increased electrostatic attraction with alien cations intercalation.[29] In the presence of 1-ethyl-3-methylimidazolium bis-(trifluoromethylsulfonyl)-imide (EMI-TFSI) ionic liquid (IL) electrolyte, in situ XRD reveals the MXene interlayer spacing increases/decreases along with negative/positive polarization, which can be ascribed to combined electrostatic attraction of $TFSI^-$ with MXene layers, and steric effect of EMI^+ intercalated in MXene layers.[6] Intercalation/de-intercalation induces lattice cell expansion/shrinkage especially on pseudocapacitive oxide electrodes. For example, the reversible expansion/shrinkage of orthorhombic Nb_2O_5 cell upon Li^+ insertion/extraction was revealed by in situ XRD, with reversible *c*-axis lattice parameter variation.[28] The crystal structure variations of MnO_2 2D birnessite in LiCl aqueous electrolyte were also studied with in situ XRD as shown in Figure 1a; the changes in lattice cells were attributable to the electrostatic attraction of intercalated cations with charged framework.[22] However, this method is non-applicable to amorphous electrode materials and requires construction of properly designed SCs that allow penetration of X-rays.

2.2. Structural Properties Variation

Aside from possible lattice shrinkage/expansion, SC electrode materials also experience other structural changes during electrochemical process, including pore structure, geometry, mass, and mechanical properties. Real time detection of the structural variations as a function of voltage in the electrochemical process can be followed in in situ X-Ray scattering, in situ AFM, in situ electrochemical dilatometry (eD), and EQCM.

2.2.1. In Situ X-Ray Scattering

Nanoporous carbon endows large surface area and copious micropores for ions adsorption and transport. In situ X-ray scattering can probe the local positions of ions and reveal the ion transportation dynamics across nanoporous carbon electrodes.[23,30] During the in situ X-ray scattering measurements, the scattered radiation of high X-ray photon flux caused by the different electron density in the electrode materials will be recorded in a temporal resolution down to seconds and milliseconds, unveiling both the changes of local ion concentration and ion location.[23,30] Using in situ X-ray scattering and Monte Carlo simulations, Presser et al. quantified the degree of ion confinement (local ion concentration variation) and desolvation in carbon materials with different pore sizes.[31] The degree of ion confinement is higher in carbide-derived carbon (CDC, pore size 0.65 nm), correlating to the higher specific capacitance

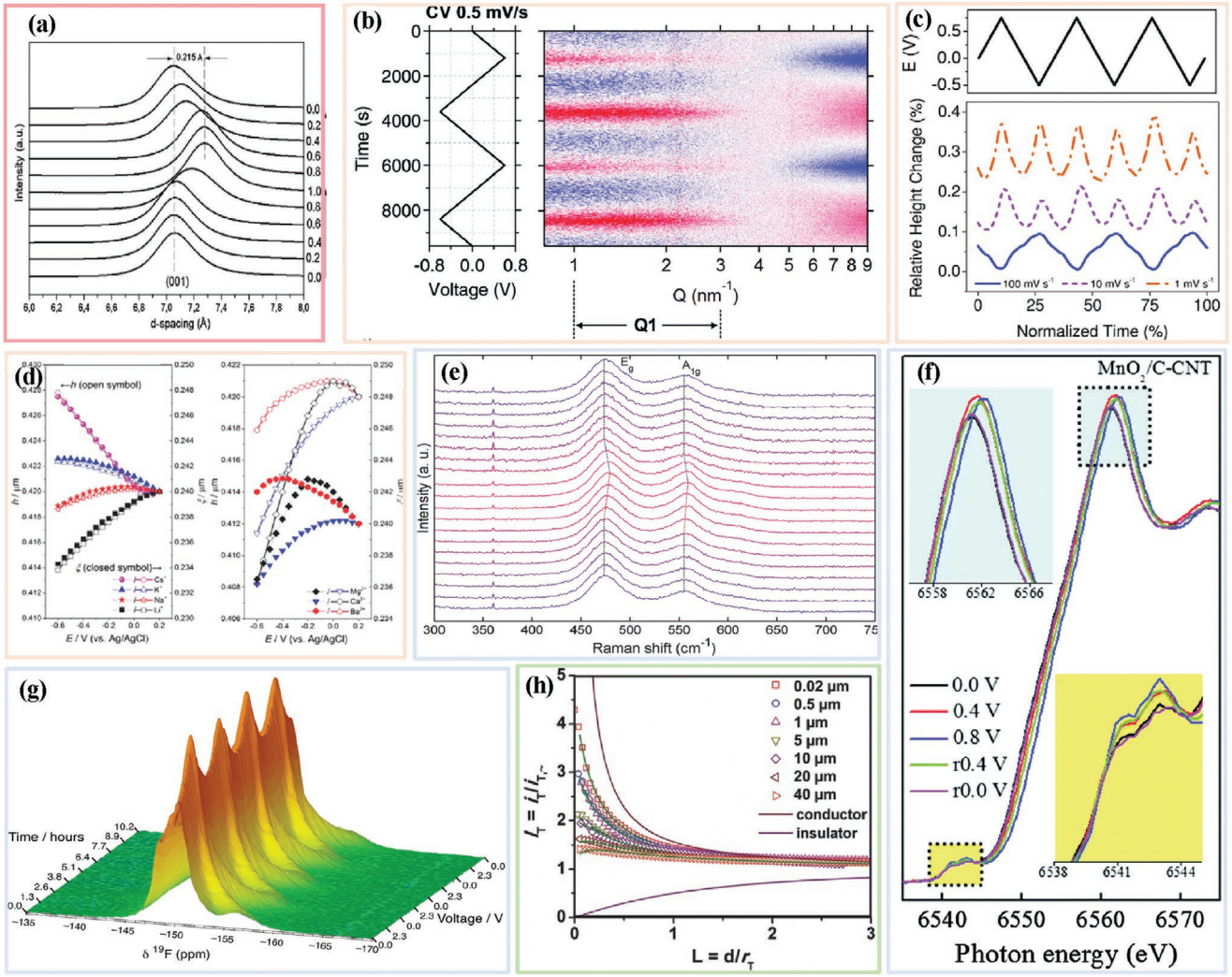

Figure 1. Representative cases of advanced characterization methods for SCs. a) In situ X-ray diffraction pattern of MnO_2 birnessite electrode in 1M LiCl electrolyte. Reproduced with permission.[22] Copyright 2012, Elsevier. b) In situ X-ray scattering of activated carbon electrode in 1 M CsCl. Reproduced with permission.[23] Copyright 2017, Royal Society of Chemistry. c) In situ atomic force microscopy measurement of mesoporous carbon in ionic liquid electrolyte at different scan rates. Reproduced with permission.[11] Copyright 2014, John Wiley & Sons. d) Electrochemical quartz crystal microbalance (with multiple overtones) measurement of Ti_3C_2 MXene in different electrolyte. Reproduced with permission.[24] Copyright 2015, John Wiley & Sons. e) In situ Raman spectra of NiO_2H_x in 2 M KOH electrolyte. Reproduced with permission.[25] Copyright 2016, John Wiley & Sons. f) In situ X-ray absorption spectra of MnO_2/C-CNT composites in Na_2SO_4 electrolyte. Reproduced with permission.[26] Copyright 2016, Royal Society of Chemistry. g) In situ nuclear magnetic resonance spectra (^{19}F) of coconut-derived carbon in ionic liquids. Reproduced with permission.[27] Copyright 2013, American Chemical Society. h) Scanning electrochemical microscopy. Approach curves of the tip to poly-aniline electrodes with different thickness. Reproduced with permission.[13] Copyright 2015, John Wiley & Sons.

(normalized to micropore volume), while partial dehydration occurred even in activated carbon (pore size 1.3 nm) with pore size larger than hydrated ions.[31] In the presence of ILs, Simon et al. employed X-ray scattering coupled with hybrid reverse Monte Carlo simulation revealing the formation of non-Coulombic ion pairs of the ILs in monolayer confinements in the nanopores of CDC (pore size 0.7 nm).[10] In situ X-ray scattering analysis further indicated the densified population of co-ions (TFSI–TFSI) in the charged pores and more EMI–EMI co-ions in discharged pores.[10] As shown in Figure 1b, in situ small angle X-ray scattering of activated carbon in CsCl electrolyte clearly demonstrated voltage-dependent local rearrangement of ions. During charging process, the degree of confinement (DoC) of cations in the pores will be increased while the DoC of anions decreases. Combination with theoretical simulation further revealed the time lag between ion transportation and voltage application, due to the accommodation of local equilibrium arrangement.[23]

2.2.2. In Situ Electrochemical Dilatometry/Atomic Force Microscopy

Macroscopic dimensional change of electrodes during electrochemical testing can be tracked by in situ eD and in situ AFM.[32,33] With construction of non-encapsulated planar SC device, the variations in mechanical properties (e.g., strain curves and elastic modulus) of the working electrode materials can also be recorded by in situ AFM when the AFM tip is in

contact mode.[9,11] Relative height changes of CDC electrodes with different pore size were monitored by in situ eD during electrochemical scans in tetraethylammonium tetrafluoroborate in acetonitrile (ACN) electrolyte.[33] With the same amount of negative charge accumulation, CDC with the smallest pore size (5.8 Å) showed maximum height change (≈2%), due to the pore expansion induced by entrance of the larger cations.[33] The volumetric expansion/shrinkage of SC electrode materials during electrochemical testing were also observed by in situ AFM.[9,11] As shown in Figure 1c, relative height change of mesoporous carbon (MC) membranes was observed by in situ AFM in IL at different scan rates.[11] Clearly, the height change is smaller at faster scan rates with only one broad peak per cycling voltammogram cycle, while larger height change is recorded with maximum/minimum height at highest/lowest potential. The strain, volume change, and ions kinetics of three types of carbon materials (MC, activated MC, and graphitized MC) with different pore size distribution and pore volumes were further studied by coupling with molecular dynamics simulation.[11] Strains will be induced during both cathodic/anodic scans with cations/anions intercalation into the small pores.[11] In order to measure the strain curves of carbon materials, a non-encapsulated planar SC was assembled, with a high surface area carbon ring as the counter/reference electrode, surrounding the working electrode at the center. During the cycling voltammogram scans, Pt-coated nanosensors AFM tip was kept in contact with the working electrode with constant contact force. The maximum cathodic strain and anodic strain for the three types of carbon materials are in the range of 0.2–0.5%. Asymmetric strain curve was observed for carbon with smallest pores (1.5 nm), with maximum anodic strain (≈0.44%) higher than cathodic strain (≈0.18%). The cations/anions kinetics were also found to be hindered by the presence of micropores.[11] On oxide nanostructured electrodes, the volume changes of MnO_2 grains during electrochemical testing were reflected by the interparticle distance variation.[9] Protons intercalation during discharge predominantly led to the expansion of MnO_2 particles, which was compromised by localized compression accompanied by reduced porosity of the electrode.[9] The height profile of 200 grains was measured and the average MnO_2 particle expansion rate was 1.9%. Some of the grains undergo shrinkage upon discharge and some undergoes expansion; on average, the grains exhibit 1.9% expansion in particle size. In addition, discharge induced softening of MnO_2 was revealed with in situ nanoindentation.[9] The nanoindentation testing was done at charged state (0.8 V, vs Ag/AgCl; Pt counter) and discharged state (0 V, vs Ag/AgCl; Pt counter); it was not stated after how many cycles was the measurement conducted. It seems the softening is more voltage-induced rather than cycling-induced.

The dimensional and mechanical properties variations during electrochemical process can be tracked by in situ AFM, yet the contact of AFM tip with electrode materials may interfere with the electrochemical reactions, and electrolyte evaporation is also possible in the open SC cells.

2.2.3. Electrochemical Quartz Crystal Microbalance

EQCM has been employed to quantify the mass change of SC electrode materials during charge–discharge process, based on the linear relation between resonance frequency and mass change as revealed by Sauebrey's equation.[14,34]

$$\Delta f/n = -C_{\mathrm{m}} \times \Delta m_{\mathrm{mass}} \tag{1}$$

In this equation, Δf is the change in the resonance frequency, n is the overtone order, C_{m} is the mass sensitivity constant, and Δm_{mass} is the mass change of electrode materials. For example, the mass of electrodeposited MnO_2 was quantified by EQCM and the coinsertion of protons and Na^+ into MnO_2 electrode during charging was verified through mass change/mole of electrode as quantified by EQCM.[35] Mass change recorded by EQCM revealed that the nanopores in N-doped carbon microspheres (pore size < 0.4 nm) are accessible for both cations and anions, harnessing high capacitance of 330 μF cm^{-2} (normalized to surface area).[36] However, linear gravimetric quantification is only conclusive when no dissipation factor (the ratio of full resonance width peak to the related resonance frequency) variation is involved.[14] In this case, hydrodynamic spectroscopy (EQCM-D) needs to be incorporated, which can operate under different overtones enabling different penetration depth.[37] The potential induced geometrical change of porous electrodes (e.g., effective layer thickness and lateral permeability length) can be derived by fitting the resonance and frequency change versus electrode potential to suitable hydrodynamic admittance model.[14,34] For example, the alkaline-ion intercalation induced MXene electrode dimension variations were extracted by EQCM-D as shown in Figure 1d, showing the increased layer distance and volume expansion of MXenes by large Cs^+ and reverse effect by smaller Li^+ with higher charge density, this occurs despite their similar cyclic voltammogram curves.[24] The frequency and dissipation factors variations of poly-pyrrole (PPy) during electro-polymerization were recorded by EQCM-D, indicating the formation of denser soft PPy microfibrils at higher deposition potential.[38] The as-obtained microfibrils PPy electrode manifests specific capacitance of ≈100 F g^{-1}.[38] With negligible viscoelastic behavior, the charging–discharging mechanism of nanoporous carbon beads (average pore size is 1.2 nm) in different ILs was studied by EQCM, revealing the involvement of smaller ions at potential close to zero charge and more favorable counterion absorption at higher potentials accompanied with electrode volume expansion.[32]

Given the above examples, EQCM-D is powerful in quantifying the mass change and geometrical variations of electrode materials during electrochemical process. However, this technique is very sensitive to the amount of electrode materials on the quartz crystal substrate, the analysis result may not be representative when the loading mass is higher. Also, the adhesion between electrode materials with the quartz crystal substrate needs to be guaranteed during testing.

2.3. Chemical Properties Variation

Other than the crystal structure and structural variations of SC electrode materials, the chemical properties changes are also of great interest. The insights on molecular structure change, oxidation states, chemical bonding, coordination chemistry, etc., are to be harvested by various methods as discussed below,

including in situ Raman/infrared spectroscopy, in situ X-ray absorption spectroscopy (XAS), and in situ NMR.

2.3.1. In Situ Raman/Infrared Spectroscopy

As a non-destructive method, in situ Raman spectroscopy can reveal valuable information of the molecular and crystal structures of electrodes during electrochemical process.[12] In situ infrared spectroscopy can also reveal chemical changes on molecular level during electrochemical testing.[39] Reversible interlayer spacing shrinkage/expansion, increased/decreased Jahn–Teller disorder, and polarizability upon discharge/charge were detected in MnO_2 birnessite with in situ Raman spectroscopy, when tested in $NaNO_3$ electrolyte.[12] Similar variations were also observed in KNO_3/$LiNO_3$, yet with higher/lower degree of disorder and polarizability upon deep discharge.[12] Charge storage mechanisms of MXene in three different sulfate electrolytes were studied by in situ Raman, revealing the bonding/de-bonding of hydronium ions with O terminals in MXene upon discharging/charging (in negative polarization) in H_2SO_4, accompanied with reversible Ti valence state change.[40] The Raman bands of MXene remain intact when tested in $(NH_4)_2SO_4$ or $MgSO_4$ electrolyte, distinguishing the ion exchange-based electrochemical mechanism in H_2SO_4 from counterion adsorption in $(NH_4)_2SO_4$ or $MgSO_4$.[40] The major contribution of O—H bonds breaking/formation to the charge storage of NiO_2H_x in alkaline KOH electrolyte was verified by in situ Raman spectra as displayed in Figure 1e, while no noticeable changes in bands features were observed in KNO_3 electrolyte.[25] Besides the aforementioned in situ Raman study of pseudocapacitive metal oxides/nitrides/hydroxides, in situ infrared spectroscopy was also employed to investigate the electrochemical process of non-Faradaic carbon materials. Entrance/exit of both cations and anions into the pores of CDC during charging/discharging was observed with in situ infrared spectroscopy.[41] For KOH activated carbon nanofibers with abundance of pores and high surface area, the charge storage mechanism of ILs in the nanopores was also revealed by in situ infrared spectroscopy, quantifying increased concentration of cations in the nanopores during charging process, which was ascribed to the increased ionophilicity by the oxygen functionalities introduced during activation process.[39]

2.3.2. In Situ X-Ray Absorption Spectroscopy

XAS is related to the transition of electrons from core levels to unoccupied electronic states, making this technique element-specific for local chemical environment detection.[26] In situ XAS can indicate the oxidation state and interatomic bonding variations in electrode materials.[26,42,43] Increased/decreased oxidation state of Mn in MnO_2 during charging/discharging was verified with in situ XAS in different pH electrolyte.[7] Larger average oxidation state change was quantified in weak acidic electrolyte than in strong acidic electrolyte, which was related to the higher pseudocapacitance in weak acidic electrolyte.[7] MnO_2-based composites also exhibit oxidation state, tunnel size, and local electronic structures variation as detected by in situ XAS.[26,44] As shown in Figure 1f, varied pre-edge absorption and main edge absorption during electrochemical testing was observed in MnO_2/C-carbon nanotubes (CNT) composite.[26] Increased oxidation state of Ni from NiO to NiOOH at around 0.5 V was revealed with absorption energy shifting through in situ XAS measurements, corroborating the anodic peak position observed in cyclic voltammogram curves.[45] Reversible average oxidation state variation of Fe in FeOOH in Li_2SO_4 electrolyte was detected with in situ XAS.[42] Decreased Fe—O and Fe—Fe bonding length upon charging was also revealed with extended X-ray absorption fine structure spectrum (EXAFS), accompanied by delithiation induced distortion relief and restored symmetry in FeO_6 octahedral unit.[42] Removal of one electron per mole of Mo in Mo_2N upon charge storage was quantified by in situ XAS, with minimal local structural variation of Mo in the EXAFS results, indicating the good structural stability.[46]

2.3.3. In Situ Nuclear Magnetic Resonance

When non-zero spin nuclei in a strong magnetic field are perturbed by a weak oscillating magnetic field, an electromagnetic signal will be produced with characteristic frequency of the magnetic field of the nucleus. The resonance frequency observed by NMR is element-dependent and sensitive to local chemical environment, making it a powerful technique for electrochemical interfaces study.[27,47] In situ NMR can detect the local chemical environment variation of elements of interest, distinguishing contribution of different chemical species to electrochemical process.[27,47] As shown in Figure 1g, in situ NMR (^{19}F, aiming at BF_4^- anions) was used to study the electrochemical mechanism of SCs based on coconut-derived activated carbon, showing periodic absorbed resonance variation.[27] Two stages of charge storage were identified, revealing the dominating short range rearrangements and co-ions ejection at voltage <0.75 V and the contribution of both counterions adsorption and co-ion ejection at voltage >0.75 V.[27] In situ NMR was also employed to study the ion dehydration process of NaF aqueous electrolyte in polymer-derived activated carbon.[48] Hydrated F^- can enter the nanopores at voltage >0.4 V while partial dehydration of F^- occurs only at voltage >0.7 V.[48] Ion diffusion coefficients (D) in nanoporous carbon (pore size < 2 nm) was quantified by in situ NMR methods with pulsed field gradient and different observation time.[8] It was found out that confinement of ions in the nanopores leads to significant reduction of D for both cations and anions, with cations suffering more drastic D reduction.[8] Deschamps et al. employed in situ 1D magnetic resonance imaging to probe the ions population variations of symmetric SCs based on CDC (pore size < 1 nm) or conventional nanoporous carbon (pore size < 2 nm). It was found out that counterion adsorption mechanism are dominating for conventional carbon, while both counterion adsorption and co-ion ejection are responsible for the higher capacitance of CDC.[47]

2.4. Electrochemical Properties

With the above-discussed characterization methods, the physical, structural and chemical variations of electrode materials

during electrochemical process can be recorded. Nonetheless, there are also approaches to gain insights on electrochemical properties of electrode materials, for example using SECM to quantify the heterogeneous charge transfer rate constants.

2.4.1. Scanning Electrochemical Microscopy

SECM system consists of a moveable ultramicroelectrode (UME, diameter < 30 μm) in a three-electrode electrochemical cell (containing redox mediator), both of which are connected to a bipotentiostat.[49,50] SECM can be utilized for both 2D mapping (feedback mode and general collection mode) and localized kinetics investigation, as well as localized surface modification.[49] SECM studies for electrochemical SCs have been carried out to provide further insights. For example, our group utilized SECM in feedback mode to quantify the heterogeneous charge transfer rate constants (k_{eff}) of MnO_2-based and polyaniline (PANI)-based electrode materials in $Fe(CN)_6^{4-}/Fe(CN)_6^{3-}$ redox mediator.[13,51] Positive feedback current from MnO_2-based electrode has been verified.[51] The approach curves of the tip to PANI electrodes with different thickness can be seen in Figure 1h, and the extracted k_{eff} values (at electrode potential of 0.6 V) correlate with the macroscopic specific capacitance, explaining the decreased specific capacitance when PANI is thicker than 5 μm.[13] Similarly, we have investigated the k_{eff} values of carbon nanotubes/hydroquinone and reduced graphene oxide/hydroquinone interfaces as quantified by SECM in feedback mode, providing further understanding for redox-active electrolyte SCs.[52] Through SECM mapping, Sapati et al. also verified the facilitated charge transfer to UME tip (biased at 0.4 V) when the electrochemically deposited MnO_2 is biased at –0.2 V.[35]

2.5. Other Properties

Aside from the above-mentioned properties variation of SC electrodes during electrochemical testing, some other phenomenon can also be observed. Heat generation in multiple carbon-based symmetric SCs were monitored during cycling, using isothermal calorimeter.[53] Identical heat generation rates in positive and negative electrodes were detected in absence of CMC (sodium carboxymethyl cellulose) binder, while presence of CMC resulted in a higher heat generation rate in the positive electrode than in the negative electrode, due to the interaction between anionic groups in CMC with the cations in the negative electrode.[53]

Gas evolution in symmetric SCs with MnO_x/reduced graphene oxide (rGO) electrode and Na_2SO_4 electrolyte was monitored with in situ differential electrochemical mass spectroscopy.[54] Evolution of CO_2 at voltage higher than 1.0 V was detected, possibly due to carbon corrosion, coincides with the working potential of the SCs.[54] Evolution of other gas (H_2, O_2) on carbon electrode in symmetric SCs at high voltages were also detected with pulsed electrochemical mass spectroscopy.[55]

The above-mentioned characterization methods for mechanism investigations of SCs have been summarized as shown in **Table 1**. The key issues of these methods, including the specific active materials, information to be derived and advantages/disadvantages have been listed. There have been a few review articles summarizing the use of different characterization methods for the mechanism investigations in electrochemical SCs.[56–59] For example, Wang et al. discussed the use of in situ XRD, in situ XAS and EQCM for mechanism investigation of SC electrodes, mostly for metal oxides and hydroxides.[58] Mai et al. reviewed the use of in situ Raman/IR spectroscopy to disclose the mechanism for carbonaceous SC materials, and the

Table 1. Summary of the key issues of the above-discussed characterization methods.

	Methods	Specific materials	Information to be derived	Advantages	Disadvantages
Crystal structure	In situ XRD	Metal oxides, MXene	Lattice parameter	Non-destructive, Fast data acquisition	Not applicable for EDLC materials and amorphous materials
Structural properties	In situ X-ray scattering	Porous carbon	Ion transportation dynamics (ion confinement, desolvation, etc.)	Non-destructive, high temporal resolution	Special set-up
	In situ eD/AFM	Porous carbon, metal oxide, etc.	Macroscopic dimensional change, mechanical properties variation	Facile set-up	AFM tip in contact with electrode materials
	EQCM	Porous carbon, metal oxide, MXene, conductive polymers etc.	Mass change, geometrical change	High sensitivity and accuracy	Loading mass on quartz crystal should be low, adhesion should be good
Chemical properties	In situ Raman/ infrared spectroscopy	Porous carbon, metal oxide, MXene, etc.	Molecular structure Crystal structure	Fast data acquisition, high spatial and temporal resolution	Possible sample heating, Localized analysis
	In situ XAS	Metal oxides, MXene, etc.	Chemical environment (chemical bonding, oxidation state coordination structure, etc.)	Applicable for both crystalline and amorphous materials	Requires high-energy X-rays with short wavelengths
	In situ NMR	Porous carbon	Local chemical environment (ion confinement)	Element-sensitive, suitable for interface study	Only applicable for non-zero spin nuclei, long sampling time
Electrochemical properties	SECM	Metal oxides, conductive polymers	Heterogeneous charge transfer rate constants	Localized investigation	Dependent on sample thickness, conductivity, porosity, etc.

use of in situ XAS and in situ XRD for metal oxide-based SC materials.[59] Zhu et al. emphasized the use of in situ IR, X-ray scattering, NMR and EQCM for SC mechanism investigation of electric double-layer capacitor (EDLC) materials.[56] In our essay, we present and distinguish the characterization methods based on the categorized information to be derived, that is, crystal structure, structural, chemical, and electrochemical properties, for both carbon-based materials and metal oxide/MXene/conducting polymers-based pseudocapacitive materials. These methods also pave the way for constructing multifunctional SCs as highlighted in this essay.

Mechanism understanding of SCs provides the basis for some of the other functions harvested by the same electrode materials. For example, the mechanical properties variation of electrode materials unveiled by in situ AFM offer instructions on the assembly of deformable SCs,[9] the structural change of electrode materials quantified by in situ XRD/dilatometry/AFM/EQCM can be related with the electrochemical actuator performances,[19] and the crystal structure variation of some metal oxides unveiled by in situ XRD is correlating with electrochromic modulation.[60] In the last section, the development of multifunctional SC will be introduced.

3. Multifunctional Applications of Electrochemical Supercapacitors

SCs were invented as energy storage devices. The understanding of the electrochemical mechanism of SCs has evolved with the help of the above-mentioned available toolkits. However, application of SCs is still limited to certain fields. The development of future electronics in different application scenarios have necessitated the integration of extra functions in SCs. Multifunctional SCs can be realized by exploring extra functions within the same SCs or by integration with other functional devices.

As displayed in **Figure 2**, SCs with multifunctionalities including but not limited to mechanical deformability, self-healability, self-chargeability, color tunability, sensing ability, and actuation have been integrated. These multifunctional SCs will certainly expand the applications of SCs and stimulate the development of future electronics with better flexibility, efficiency, and sustainability. Multifunctional SCs demonstrated in literature will be presented and discussed as follows.

In order to construct multifunctional SCs, one need to carefully evaluate different electrode materials, electrolyte, current collector, and substrates for different purposes.[61–63] a) For the electrode materials, carbon-based EDLC materials manifest high electrical conductivity, high porosity, and high electrochemical stability, thus fast discharge and high power density, while the capacitance and energy density are often limited. Pseudocapacitive materials (e.g., metal oxides, MXene, and conductive polymers) based on Faradaic reactions have better charge storage capability, at the expense of discharge rate and power. In addition, carbon-based materials often offer better mechanical stability and can be used as backbone to support pseudocapacitive materials, harvesting the merits of both.[62] b) Electrolytes used for SCs include aqueous-, organic-, and IL-based electrolytes. Aqueous electrolytes have high ionic conductivity (10^1–10^2 mS cm^{-1}) yet narrow voltage window. Organic electrolyte can sustain wider voltage window (up to 3.5 V), with sacrificed ionic conductivity (10^0–10^1 mS cm^{-1}). IL-based

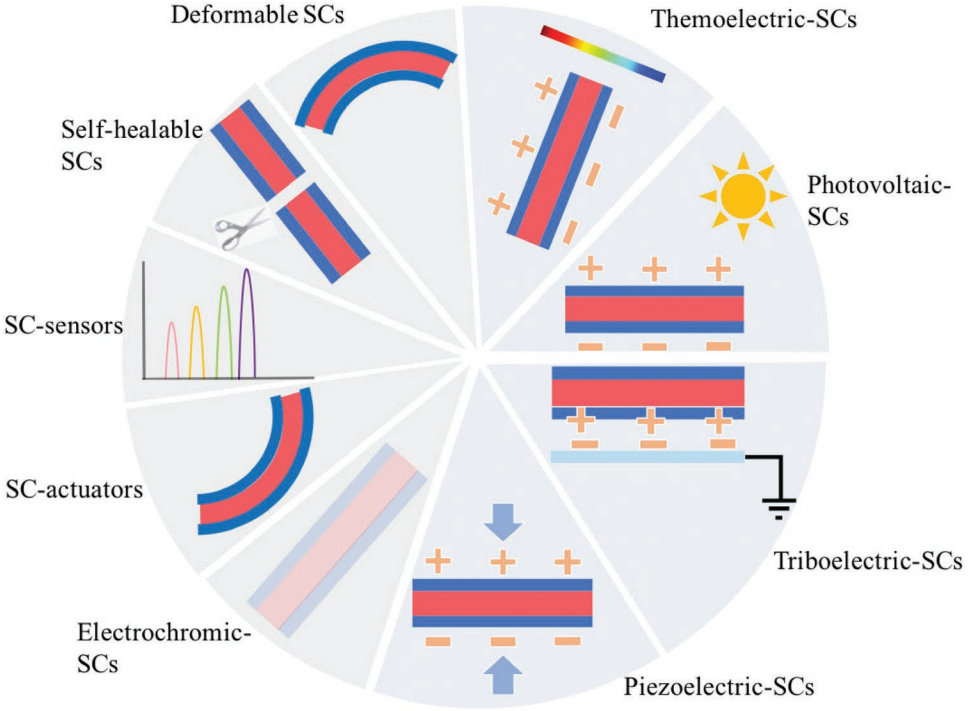

Figure 2. Schematic illustration of multifunctional supercapacitors, including mechanically deformable, self-healable SCs, SC-sensors, SC-actuators, electrochromic SCs, and self-chargeable SCs (piezoelectric-, triboelectric-, photovoltaic-, thermoelectric SCs).

electrolytes have the merits of low vapor pressure and good electrochemical stability (operational voltage up to 3.7 V), while the high viscosity and low ionic conductivity will cause limited rate performance.[62] During SC assembly, liquid electrolyte can often lead to electrolyte leakage. Incorporation of polymer host in aqueous and/or organic electrolyte, and fumed silica in ILs can resolve the electrolyte leakage issue and avoid the use of separator, while allowing good mechanical stability and flexibility. Again, the ionic conductivity will be sacrificed and proper sealing still needs to be guaranteed. c) The current collector/substrate is also of great importance for multifunctional SCs assembly. Rigid substrates, for example, silicon wafer and ITO/fluorine-doped tin oxide (FTO) glass are not applicable for deformable SCs, while polymer-, paper-, and textile-based substrates are favored in this case. For multifunctional electrochromic SCs, substrates with high transparency is needed to allow light modulation.[61]

3.1. Deformable Supercapacitors

SCs with rigid structures are limited and unfavorable for wearable electronics, portable electronics, flexible displays, etc., triggering efforts to develop mechanically deformable SCs.[2] Preparation of flexible SCs are mostly relied on the assembly of flexible electrodes, which are normally realized by using conductive carbon materials or metals as substrate/current collector.[64,65] Flexible SCs based on only carbon materials, for example, activated carbon, carbon nanotubes, and graphene fibers as electrodes have been extensively studied. Wei et al. mixed CNT with activated carbon, obtaining activated carbon/CNT flexible electrode with specific capacitance of 267.6 F g^{-1}.[66] Fiber-shaped carbon-based electrodes was also developed for flexible SCs. Wire-shaped SCs based on symmetric CNT/ordered MC fiber electrodes and PVA (polyvinyl alcohol)/H_3PO_4 gel electrolyte was developed.[67] The SC wires has optimized specific capacitance of ≈2 mF cm^{-1}, without significant capacitance decay after 1000 cycles' bending.[67] Similarly, activated carbon drop-casted onto carbon fibers and PVA-H_3PO_4 gel electrolyte were used to fabricate fiber-shaped symmetric SCs, which realized specific capacitance of 45.2 mF cm^{-1}.[68] Three SCs were weaved into a wrist band and can light up an LED.[68] Wet-spun graphene fibers was coated with PVA-H_2SO_4 gel electrolyte, which was further coated with sheath graphene fiber and the same gel electrolyte, fabricating a fiber-shaped SC.[64] Specific capacitance of 182 F g^{-1} was realized by the SC, which can be weaved into cotton yarn with capacitance retention of 92% over 100 bending cycles.[64]

Flexible SCs incorporating pseudocapacitive materials are favorable in terms of specific capacitance and energy density. MnO_2 was electrodeposited onto CNT paper, obtaining flexible electrode with specific capacitance of >150 F g^{-1}.[69] PANI polymerization on CNTs was also conducted to obtain flexible paper electrode, which was soaked in PVA-H_2SO_4 gel electrolyte to fabricate symmetric ultrathin SCs.[70] The paper SC have thickness comparable to A4 paper and capacitance of 150 F g^{-1} for the whole device.[70] Electro-polymerization of PANI onto graphene paper also produced flexible SC electrode.[15] Asymmetric flexible SCs employing CNT paper as current collectors for both electrodes were fabricated. MnO_2 electrodeposited onto CNT paper and PANI electropolymerized on CNT paper are the positive and negative electrodes, respectively, which were further assembled into flexible SCs with polyvinylpyrrolidone (PVP)-Na_2SO_4 gel electrolyte.[71] The flexible SCs showed maximum energy density of 24.8 Wh kg^{-1}.[71] Flexible fiber-shaped SCs using symmetric bisrolled CNT/poly(3,4-ethylenedioxythiophene) (PEDOT) yarns as electrode with PVA-H_2SO_4 gel electrolyte was fabricated, showing excellent mechanical deformability with no obvious capacitance degradation after 10 000 cycles at bent state.[72] Instead of CNTs or graphene paper, metal substrates were also utilized to fabricate flexible SCs. $ZnCo_2O_4$ grown on Ni foam was used as the electrode for symmetric flexible SCs with PVA-KOH gel electrolyte.[65] The flexible SC showed excellent capacitance retention of ≈100% over 3000 cycles at bent or twisted states.[65] Other than directly utilizing conductive substrates, modification of originally non-conductive substrates to obtain conductive and flexible substrates have also been reported. CNTs absorption onto cellulose sponge[73] and infiltration into Kimwipes tissues[74] result in conductive and flexible substrates, which were utilized for MnO_2 electrodeposition and PANI polymerization, respectively. Polyester cloth coated with reduced graphene oxide was also utilized as conductive and flexible substrate for PANI polymerization, enabling fabrication of flexible and wearable SC fabrics.[75] The flexibility of the above-mentioned flexible SCs are realized through different strategies. i) adoption of flexible/conductive substrate, for example, CNT paper, graphene paper, and Ni foam.[15,65,69] ii) Incorporation of gel electrolyte, for example, PVA-H_3PO_4.[67] iii) SCs with different form factor, for example, fiber-shaped.[67]

Aside from flexibility, stretchable SCs are also required for certain applications. Fabrication of stretchable SCs are more challenging than assembly of flexible SCs, with the "prestraining" approach often adopted.[76] SCs based on electrodes of PANI electrodeposited on wavy graphene foam sustained stretchability of 20%,[77] while stretchability of 370% was obtained in SCs based on electrodes of prestretched elastic fiber wrapped by aligned CNT arrays.[78] Elastomeric substrates are also often used for fabrication of stretchable electrodes.[79] Electrode of laser-induced graphene on polydimethylsiloxane (PDMS) showed stretchability of 50%.[80] Electrode of CNT arrays fixed by polyurethane (PU) manifests stretchability of 500%.[81] Symmetric SCs fabricated using this electrode and PVA-H_3PO_4 can sustain stretching of 200% with minimal capacitance degradation.[81] Our group has attempted to fabricate stretchable SCs using Ag-wire networks embedded in PU acrylic substrate as the current collector.[82] Electrochemical coating with Ni and Fe onto Ag nanowires (NWs) results in the positive and negative electrodes, enabling fabrication of asymmetric SCs with stretchability of 35% and transparency (50%).[82] In a nutshell, assembly of stretchable SCs are often relying on the "wavy" structure, "prestraining" approach, and elastomeric substrate, with the use of gel electrolyte.[62]

3.2. Self-Healable Supercapacitors, Shape Memory Supercapacitors

Repeated deformations may cause accidental damage of SCs and performance degradation in practical applications,

necessitating the development of self-healable SCs and shape memory SCs (SMSCs) with extended life span.[16,83,84]

Self-healable electrodes through incorporation of self-healing polymers (SHPs) have been developed. The SHPs can be obtained based on Leibler's method.[85–87] This method employs carboxylic-acid ends to attach functional groups (amidoethyl imidazolidone, di(amido ethyl)urea, and diamido tetraethyl triurea), forming SHPs based on multiple hydrogen bonds.[88] The structure stability of PANI/GO electrodes was improved by hydrogen-bond-based SHPs coating, leading to increased cycling life (≈97.5% capacitance retention after 9000 cycles) of the full SCs device.[85] Wrapping aligned CNTs on SHP fibers resulted in the self-healable electrodes, enabling fabrication of self-healable wire-shaped SC device.[87] TiO_2 nanospheres incorporated SHPs were employed as self-healable substrates for spreading of CNTs, allowing the assembly of symmetric SCs with PVP-H_2SO_4 gel electrolyte.[86] Our group also developed a self-healable substrate based on liquid metal particles on carboxylated PU (CPU).[89] Further coating of graphene platelets enables assembly of stretchable and self-healable symmetric SCs with IL electrolyte. The self-healing process was based on the hydrogen bonding of CPU and the flow of liquid metals.[89] Thermally self-healable substrates based on Ag NWs on polycaprolactone (PCL)/PVA was developed.[90] Thermal induced softening of PCL/PVA enables the restoration of the electrical conductance between Ag NWs.[90] Magnetic-assisted self-healable yarn SCs were assembled with PPy/magnetic Fe_3O_4/stainless steel fiber electrodes and PVA-H_3PO_4 gel electrolyte.[83] SHP CPU was used to coat the whole symmetric yarn SCs. Under magnetic field, the magnetic fibers will reconnect, restoring 71.8% of the electrochemical performance of the yarn SCs after four times breaking/healing.[83]

Self-healable electrolytes based on hydrogels or ionogels were also synthesized for self-healable SCs.[91] Self-healable supramolecular hydrogel electrolyte based on KCl-Fe^{3+}/poly acrylic acid (PAA) was developed with ionic conductivity of 0.09 S cm^{-1}, endowing higher cycling stability in SCs as compared to liquid electrolyte.[92] The self-healing property was based on the formation of interchain bonding between PAA and Fe^{3+} at the cut interface.[92] Sodium alginate grafted with dopamine/KCl hydrogel electrolyte is also self-healable based on the dynamic catechol—borate—ester bonding, enabling self-healable SCs sustaining ten cycles of cut/healing.[93] Polyelectrolyte was synthesized by PAA dual crosslinked by hydrogen bonding and vinyl hybrid silica nanoparticles, endowing as-fabricated self-healable SCs with >100% healing efficiency after 20 breaking/healing cycles.[16]

SMSCs have been demonstrated in literature with incorporation of shape memory polymers or alloys as substrates.[84,94–96] With coating of aligned CNTs on shape memory PU fibers, fiber-shaped symmetric SMSCs can be obtained with PVA-H_3PO_4 electrolyte, maintaining electrochemical performance during deformation and after shape recovery.[95] NiTi shape memory alloy was used as both substrate and current collectors to fabricate SMSCs.[84,94] Yan et al. utilized graphene on NiTi as negative electrode and MnO_2 on Ni film as positive electrode to fabricate SMSCs.[94] The NiTi alloy has phase transition temperature of 15 °C, thus human skin temperature can actuate the shape recovery of the SMSCs.[94]

3.3. Low-Temperature Supercapacitors

In extreme weather conditions, for example high altitudes and cold climates, the advantage of high power density of electrochemical SCs will be significantly compromised due to the increased equivalent series resistance and electrode ionic resistance, especially in aqueous and propylene carbonate (operating limit −25 °C)-based electrolyte.[97,98,99] In order to construct low-temperature-tolerant SCs, alternative electrolytes with mixed salts/solvents have been developed.[98]

Hydrogel-based electrolytes with abundant hydrogen bonding between hydrophilic polymer chains with water molecules can effectively disrupt ice formation, thus improving the low-temperature performance of SCs.[100,101] With dual-crosslinked PVA-AA-H_2SO_4 hydrogel electrolyte, the specific capacitance of a symmetric SC based on MoN/CNT electrodes can retain 80% of its original value after being stored at −35 °C for 23 days.[100] Incorporation of fatty species was also attempted to improve the antifreezing properties of PVA hydrogels.[102] The storage modulus of LiCl-PVA-H_2O hydrogel was increased dramatically when the temperature was reduced from 25 to −40 °C, while the storage modulus of LiCl-PVA-H_2O/ethylene glycol hydrogel remain almost constant. As a result, symmetric SC employing this LiCl-PVA-H_2O/ethylene glycol hydrogel electrolyte and CNT paper electrodes can maintain 88.3% of its capacitance even after 5000 cycles at −20 °C.[102]

Super-concentrated water-in-salt electrolyte (WiSE) exhibit wide electrochemical window of ≈3 V due to the strong coordination of water molecules with the Li^+.[103,104] However, the tendency of salt precipitation in these WiSE electrolytes at low temperatures will inevitably exclude their application in low-temperature scenarios.[103,104] In view of this, Yan et al. blended ACN solvent with WiSE to formulate AWIS electrolyte, endowing increased ionic conductivity, reduced viscosity, and preserved voltage window. The incorporation of ACN molecules can disrupt the cation–anion aggregates due to spatial isolation while preserving the strong coordination of water molecules with Li^+ in LiTFSI-based AWIS electrolyte.[103] Similarly, in $NaClO_4$-based AWIS electrolyte, ACN molecules strongly coordinates with Na^+, changing the solvation structure from cation–anion aggregates to contact ion pairs (one ClO_4^- anion coordinate with one Na^+) and/or solvent separated ion pairs.[104] In this $NaClO_4$-based AWIS electrolyte, commercial activated carbon can maintain 86.5% of its room-temperature capacitance at −50 °C.[104]

Low ice point ILs were also employed as electrolytes to assemble temperature-tolerant SCs. For example, symmetric SCs with lamellar porous carbons tack electrodes and 1-butyl-3-methylimidazolium tetrafluoroborate (ice point of −72 °C) electrolyte were assembled, exhibiting specific capacitance of 76.8 and 25.2 F g^{-1} at 20 and −30 °C, respectively.[99] Mixing ILs with binary organic solvents was also attempted to decrease the viscosity of ILs at low temperature without narrowing the electrochemical window.[105–107] Yan et al. reported a 1-butyl-3-methylimidazolium tetrafluoroborate/ACN/methyl acetate-based electrolyte, which manifest widened potential window of 3.5 V at −50 °C.[105] Symmetric SCs employing this electrolyte and PANI derived activated carbon electrodes

delivered specific capacitance of 45 F g^{-1} at −50 °C, comparable to that at room temperature, with capacitance retention of 71.2% after 10 000 cycles at −50 °C.[105] Similarly, Ding et al. reported a low melting point triethylmethylammonium tetrafluoroborate/ACN/1,3-dioxolane electrolyte.[106,107] Sluggish ion desolvation at low temperature will lead to drastic decay in capacitance when the pore size of activated carbon is <0.9 nm. On the contrary, temperature independent capacitance can be manifested in activated carbon electrode with pore size of >0.9 nm, delivering specific capacitance of 164 F g^{-1} at −100 °C.[106]

3.4. Supercapacitors-Sensors

SCs with high power density and long cycling life are ideal power sources for digital communication electronics.[108] Various sensors, including photodetector,[109] chemical sensor,[110,111] strain/pressure sensor,[112,113] and temperature sensor,[114] integrated with SCs have been demonstrated. Shen et al. reported a self-powered photodetector system based on in-plane SCs of $GeSe_2$/PVA-H_2SO_4/$GeSe_2$ powering photodetectors of CdSe NWs, giving similar current response on white light illumination when the photodetector is powered either by the SCs or external power of 0.3 V.[108] Instead of directly connecting SCs with sensors, higher level of integration of SCs and photodetectors into one device were also realized by employing light-sensing materials as electrode for SCs.[115] Graphene was used as both the negative electrode for SCs and the light-sensing material, realizing photodetection through monitoring the leakage current of SCs.[115] Similarly, TiO_2-based integrated SC-photosensor in one device was also realized by monitoring leak current of SCs.[20] Chemical sensors based on SC electrodes have been showcased in literature. Graphene/ZnO electrode has lower detection limit of ≈1.0 μM and ≈10 nM for $[Fe(CN)_6]^{3+}$ and dopamine, respectively.[110] Hierarchical SnO_2 nanostructures showed conductance variation to multiple volatile gases exposure, with highest response to ethanol.[111] Specific capacitance of 187.7 F g^{-1} was also realized by the same electrode.[111] $ZnCo_2O_4$/PANI composite electrode delivers capacitance of 398 C g^{-1} while realizing hydrazine sensitivity of 0.43 μA $μM^{-1}$ with lower detection limit of 0.2 μM.[116] NO_2 sensor based on graphene and microSCs based on PANI/CNT was integrated on the same deformable substrate, realizing stretchable self-powered gas sensor.[117] Aside from photo- and chemical-sensors, other type of sensors integrated with SCs have also been attempted. CNT-PDMS sponge manifests high sensitivity (0.008 kPa^{-1}) as piezo-resistive sensor,[113] which can also be employed as electrodes for symmetric SCs. The symmetric SCs show volumetric capacitance of 13.82 mF cm^{-2}.[113] 3D printed fiber-shaped SCs based on V_2O_5/CNT and VN/CNT electrodes were integrated with temperature sensors based on rGO fibers, realizing self-powered integrated fiber-shaped temperature sensor with sensitivity of 1.95% $°C^{-1}$.[114] SCs integrated with multiple sensors were also demonstrated, utilizing PPy coated on CNT stretchable textile as both light-sensing and pseudocapacitive electrodes.[112] In this self-powered device, both energy storage SCs, photosensors and strain sensors are integrated.[112]

3.5. Supercapacitor-Actuators

Actuators can convert external stimuli (heat, electricity, light, etc.) into mechanical energy with deformations or motions for soft robotics.[19,118] Carbon-based materials with high surface area and high electronic conductivity have been widely reported for both actuators and SCs. Aabloo et al. reported a bifunctional SC-actuator based on CDC electrode in IL electrolyte, which delivers maximum strain of 0.6% and gravimetric capacitance of 119 F g^{-1}.[119] The actuation mechanism was related to the different ion size effect.[119] Incorporation of Fe_3O_4 nanoparticles into graphene layers was found out to increase the actuation strain by 56% due to the mitigated restacking, while harnessing specific capacitance of ≈65 F g^{-1}.[120] The actuation phenomenon was dominated by Coulombic contribution.[120] Recently, Gao et al. reported a bifunctional symmetric SC-Actuator device based on MXene electrode with gel electrolyte PVA-H_2SO_4, which can accumulate curvature of 0.038 mm^{-1} and strain of 0.26% as well as capacitance of 55 F g^{-1}.[19] The actuation is caused by proton insertion/extraction induced interlayer spacing expansion/shrinkage of MXene, as revealed by in situ XRD analysis.[19] Instead of ion insertion/extraction induced actuation, bifunctional SC-actuators based on joule heating was also reported. Graphite paper deposited with PANI nanoparticles was laminated with biaxially oriented polypropylene (BOPP) film.[118] The different thermal expansion coefficient between BOPP and graphite paper resulted in the actuation upon voltage induced joule heating. The graphite paper-based electrode demonstrates large bending curvature (1.03 cm^{-1}) at a low driving voltage of 2.5 V and areal specific capacitance of 402.5 mF cm^{-2}.[118] Integrated bifunctional SC-actuator devices based on this electrode was demonstrated as a gripper with charge storage capability.

3.6. Electrochromic Supercapacitors

Electrochromism happens when the electrode materials are biased in electrolyte, accompanied by electrochemical ion insertion/extraction, resembling the electrochemical process in pseudocapacitors.[2,17,60] Inspired by the similarity between EC and SC, bifunctional SC-EC devices have been demonstrated in literature. Yang et al. reported a multifunctional SC-EC window by employing WO_3 on FTO glass as electrode through thermal evaporation.[121] A high specific capacitance of 639.8 F g^{-1} and a large transmittance modulation of 76.2% are both harvested by the as-prepared electrode. In WO_3-based SC-EC device, the transmittance modulation was achieved by the reversible oxidation state change of W center between W^{6+} (transparent state) and W^{5+} (colored state), accompanied by charge storage/release.[61] Thus, the charge/discharge state of SC-EC device can be visually inspected based on the color.[61] SC-EC bifunctional cells based on WO_3 quantum dots,[122] other metal oxides including NiO,[123] $NiMoO_4$,[124] and V_2O_5,[125] or conducting polymers[126] have also been reported. Instead of relying on rigid FTO/ITO glass-based substrate, mechanically deformable SC-EC devices have also been achieved by adoption of different conductive substrates. For example, WO_3 was electrodeposited onto flexible polyethylene terephthalate (PET)/Ag

grid/PEDOT: PSS films, which achieved optical modulation of 81.9% with specific capacitance of 221.1 F g^{-1} (at current density of 1 A g^{-1}) in 0.5 M H_2SO_4.[127] Other flexible SC-EC devices based on $Ni(OH)_2$ on Ag NWs/PEDOT: PSS/poly(ethylenimine) ethoxylated,[128] PANI on PEDOT/PET,[129] PANI on Au NWs membrane,[130] PANI on ITO/PET,[131] polyFe on ITO/PET,[132] etc., have also been prototyped in literature. Fiber-shaped SC-EC bifunctional device utilizing PANI on CNT/elastic fiber[133] and stretchable SC-EC devices based on WO_3 nanotubes on Ag NWs/PDMS[134] have been reported as well.

3.7. Self-Chargeable Supercapacitors

Energy conversion devices that convert energy from environment into electric energy have emerged as intriguing devices to improve energy efficiency. However, the converted energy is normally intermittent and dependent on the environmental conditions, thus storage of the converted electric energy is desired. In this section, integration of SCs with solar cells, piezo-, tribo-, and thermo-electric devices will be showcased and discussed.

3.7.1. Solar Cells Supercapacitors

Solar cells can only convert solar energy into electric energy during daytime, thus integration with energy storage devices, for example, SCs, is a necessity.[135] Gong et al. attempted to power a flexible solid state SCs with perovskite hybrid solar cells (V_{oc} of 0.9 V).[135] The SCs can be charged to 0.75 V and sustain a discharge time of 45 s (at 1 A g^{-1}).[135] Wang et al. demonstrated a power pack composed of a perovskite solar cell ($CH_3NH_3PbI_3$-based) and a SC (PPy-based) connected in series.[136] The power pack delivered high energy storage efficiency of 10% and has an improved output voltage of 1.45 V under AM 1.5G illumination when SC is fully charged.[136] With the purpose of device miniaturization and footprint area reduction, photo-capacitor devices, in which solar cells and SCs have one shared electrode, have been developed. For example, Peng et al. demonstrated an energy fiber with solar cells and SCs at two ends, sharing the same Ti wire.[18] The energy fiber gives total photoelectric conversion to storage efficiency (η) of 0.82%, and are flexible and weavable.[18] Wang et al. reported a power unit composed of a hybrid silicon NW/polymer heterojunction solar cell and a PPy-based SC using Ti film as the conjunct electrode, yielding η value of 10.5%.[137] Furthermore, both photo conversion and energy storage capabilities can be integrated into a single device.[138] A bifunctional twisted fiber consisting of $Ti@TiO_2$ fiber as the core and CNTs/PANI as the shell, separated by electrolyte containing I_3^-/I^- redox ion couple, has been prototyped.[139] The twisted fiber demonstrated high energy conversion efficiency of 6.58% and specific capacitance of 85.03 mF cm^{-1}.[139]

3.7.2. Piezoelectric Supercapacitors

Piezoelectric devices harvest mechanical energy into electric energy, which is intermittent if the mechanical input is non-continuous.[140] Taking polarized poly(vinylidene fluoride) (PVDF) film as an example, the piezoelectricity originates from the β-phase where C-F dipoles are aligned in the same direction, creating intrinsic charges.[61] Desirable piezoelectric-SCs (PESC) devices that store intermittent electric energy have been attempted and showcased in literature. Wang et al. reported a self-chargeable PESC device based on MnO_2 electrode sandwiching PVDF-ZnO piezoelectric separator immersed with H_3PO_4-PVA electrolyte.[141] The PESC device can be charged to 110 mV with human palm impact within 300 s.[141] Our group demonstrated a bifunctional PESC device based on poled porous piezopolymer (poly[vinylidene fluoride-co-trifluoroethylene]) foam immersed with $LiClO_4$-based gel electrolyte, sandwiched by CNT electrodes.[142] Upon application of mechanical force, as-generated piezoelectric potential creates ion concentration gradient in the electrolyte, increasing the open circuit potential (OCP). With mechanical force of 70 N at 5 Hz, the OCP can be improved by 70 mV, with capacitance of 95 μF cm^{-2}.[142] Similarly, bifunctional PESCs based on porous electrospun piezoelectric separator immersed with ion gel electrolyte, and subsequently sandwiched with $MoSe_2$ electrodes was reported.[143] The device can be charged to 708 mV with mechanical force of 30 N within 100 s.[143] Bifunctional PESC device with asymmetric electrodes was also designed to enlarge the voltage operation window.[144] Hydroxide-based cathode and rGO-based anode with PVA-KOH electrolyte were incorporated, with perforated fish swim bladder as the piezoelectric separator.[144] The OCP of the device can be increased by ≈150 mV within 80 s by finger imparting at 1.65 Hz. Energy storage capability of the device has been demonstrated by powering LEDs and small electronic gadgets.

3.7.3. Triboelectric Supercapacitors

Triboelectric nanogenerators (TENG) can convert mechanical energy into electric energy through coupled contact electrification and electrostatic induction.[145,146] Integration of TENG and SC devices have also been attempted.[146,147] Wang's group has paid much efforts in developing deformable integrated bifunctional TENG-SC devices for portable and wearable electronics.[148–150] For example, fiber-shaped symmetric SC based on rGO/Ni/polyester yarn electrodes and PVA/H_3PO_4 gel electrolyte can be powered by TENG fabrics of weaved intercrossed Ni/polyester and parylene/Ni/polyester straps versus common cotton cloth.[150] The SC (three connected in series) can be charged to 2.1 V by the textile-based TENG in 2009 s with vibration motor at 5 Hz, demonstrating dual-functionality.[150] Paper deposited with Au was utilized as substrates for electrodes of both SCs and TENGs, enabling the assembly of ultralight and deformable rhombic-shaped TENG-SC device.[149] Laser-induced-graphene on both sides of polyimide film was used as electrode for SC and TENG separately, allowing the assembly of bendable TENG-SC into one device.[145] Stretchable and washable TENG-SC bifunctional devices were also realized through weft-knitting of fiber-shaped TENG and SCs, realizing maximum peak power density of ≈85 mW cm^{-2} and lighting up 124 LEDs at stretched state.[151] The TENG consists of stainless steel/polyester yarns coated with silicone rubber while the SC is based on symmetric PEDOT:PSS/CNTs/carbon fiber electrodes in PVA/H_3PO_4 gel electrolyte.[151]

3.7.4. Thermoelectric Supercapacitors

Thermoelectric devices harvest thermal energy into electric energy through Seebeck effect, usually based on thermodiffusion of electronic charge carriers.[152,153] Nonetheless, ionic thermoelectric devices based on thermodiffusion of ionic charge carriers (Soret effect) are also being investigated.[152,153] Kim et al. utilized a thermoelectric device to power a SC, achieving discharging/charging ratio of 98% with eliminated Soret effect.[154] Crispin et al. reported an integrated thermoelectric-SCs bifunctional devices employing symmetric CNT/Au electrodes with poly(ethylene oxide) (PEO)-NaOH electrolyte, inducing Na^+ and PEO^- concentration gradients upon thermal gradients, storing the thermo-induced electric energy in SCs.[155] The integrated thermoelectric-SC bifunctional device has much higher conversion efficiency compared to a typical thermoelectric and SC devices connected in series.[155] The same group also studied the conversion efficiency of polystyrene sulfonate sodium ($PSS-Na^+$) electrolyte, for the application of ionic thermoelectric SCs.[152] Similarly, Yu et al. utilized polystyrene sulfonic acid electrolyte and PANI/Graphene/CNT electrode to fabricate an ionic thermoelectric-SC device, realizing charged potential of 38 mV and areal capacitance of 120 mF cm^{-2} upon temperature difference of 5.3 K. An increased OCP in SCs was also observed when being heated up to 65 °C, which is attributed to the enhanced Faradic kinetics at the electrode surface.[156]

3.8. Multifunctionality

Dual-functionality is not the destination for SCs development, integration of multiple functions with SCs is also being pursued. Kim et al. fabricated a self-powered human-activity sensor by integrating TENG with SC.[157] The TENG is with two electrodes, the patterned PU/polyimide on conductive carbon fabric and patterned PDMS/Al on carbon fabric. The TENG harvests the mechanical energy produced during the swing motions, powering the SCs composed of CNT/RuO_2 electrodes.[157] The slope of charge accumulation by the TENG is linearly proportional to the frequency of rubbing, enabling monitoring of human activity, demonstrating an integrated wearable self-powered human activity monitoring system.[157] Wang et al. reported a self-powered pressure sensor system, by integrating ultrathin SCs based on A4 paper and ultrathin TENG based on ITO and polytetrafluoroethylene films. Electricity generated by TENG can be stored by SCs, and the voltage of SCs increases with higher pressure applied, enabling a biomimetic self-powered pressure sensor system that can detect both static (detection limit 0.07 N cm^{-2} and sensitivity of 12.1 mV cm^2 N^{-1}) and dynamic pressure (detection limit 0.3 N cm^{-2} and sensitivity of 17.5 V cm^2 N^{-1}).[158] Another self-powered pressure/temperature sensor was also realized by coupling piezoelectric PVDF into separator of solid-state SCs.[159] The capacitance of SCs are increased with higher temperature and static pressure. The integrated sensor can detect both static (detection limit 0.1 N cm^{-2} and sensitivity of 2.47 nF cm^2 N^{-1}) and dynamic pressure (detection limit 0.4 N cm^{-2} and sensitivity of 15.5 mV cm^2 N^{-1}) sensing as well as temperature (sensitivity of 0.1521 nF cm^2 $°C^{-1}$).[159] Smart cloths that can convert solar energy and body motion energy into electricity by fiber-shaped dye-sensitized solar cell ($TiO_2//I_3^-I^-//C@Pt$) and fiber-shaped TENG (Cu vs PDMS), and store the energy in fiber-shaped SCs (symmetric $RuO_2 \cdot xH_2O$ electrodes in PVA-H_3PO_4) were prototyped by weaving the three fiber-shaped devices.[160] This smart self-chargeable textile is a good example of applying integrated SCs for wearable electronics.

4. Summary and Perspectives

With adoption of various characterization techniques, the properties variation of SCs electrode materials can be monitored. Electrochemical charge/discharge induced crystal structure expansion/shrinkage, ion confinement in nanopores, induction of strain, dimension expansion/shrinkage, chemical bonding formation/breakage, oxidation state increase/decrease, etc., have been observed. Representative case studies have been summarized in Figure 1. However, for different electrode materials the characterization methods need to be carefully selected. Some of the methods are favorable for carbon electrode materials based on non-Faradaic reactions, for example, in situ NMR, X-ray scattering to study the ion diffusion dynamics, including ion desolvation, confinement, and local rearrangements in nanopores. Some of the methods are more suitable to study metal oxides-/carbides-based electrode materials involving Faradaic reactions, for example, in situ XRD and XAS to monitor the crystal structure, chemical bonding, and oxidation state variations. Nonetheless, some methods are applicable for both types of materials, for example, in situ eD, AFM, EQCM, and SECM to monitor the dimensional and electrochemical properties variation. Thus, it is suggested to evaluate the strength of respective methods before employing these tools for analysis in specific cases, and combination of more than one method is needed sometimes. Theoretical calculation/simulation is also informative and can complement experimental characterization methods, yet this aspect is not covered in this essay.

"Self-discharge" phenomenon in SCs will cause spontaneous voltage drop and capacitance decay under the OCP, which is the bottleneck and detrimental to the wide adoption of SCs.[161,162] However, the "self-discharge" mechanism is not fully understood. Theoretically, some of the toolkits discussed in Section 2 can be employed to better unveil the self-discharge mechanism. As listed in Table 1, in situ Raman/IR spectroscopy, in situ X-ray absorption spectra, in situ NMR, etc., can be employed to monitor the change in surface chemical bonding of electrode under OCP; in situ X-ray scattering can be adopted to monitor the variation of pore structure under OCP. For example, the mitigated self-discharge rate in thermally annealed $Ti_3C_2T_x$ was correlated with the lower valence state and higher coordination number of Ti after eliminating F atoms, as evidenced by XANES spectra.[162] The anti-self-discharge phenomenon of few-layer phosphorene (FLP)-based hybrid Zn-ion capacitor was also correlated with the reduced A_g^1(large component in the direction of armchair outside of the plane)/B_{2g} (mode moves along the serrated direction inside the plane) ratio of FLP at the discharged state, as revealed by Raman mapping.[163] However, as far as we know, the number of publications in this topic is still quite limited, more efforts are to be spent to disclose the

self-discharge mechanism in SCs with the available characterization methods.

Multifunctional SCs have been demonstrated as schemed in Figure 2. However, the electrochemical performance of these SCs should be maintained or at least not severely sacrificed. Novel design in electrodes/electrolytes/current collectors/configurations will inevitably increase the weight and dimension of the full SCs, compromising the gravimetric/volumetric capacitance. Incorporation of heavy current collectors, SHPs, or shape memory alloys, etc., to construct deformable, self-healable, and shape memory SCs is not favorable when lightweight is required. The actuation in integrated SC-actuators will also be mitigated when incorporating heavy components. Color tunable SC-ECs employing heavy ITO/FTO glass also suffered from low gravimetric capacitance. The energy conversion efficiency in self-chargeable SCs harvesting solar-, piezo-, tribo-, thermo-electric energy needs to be improved.

Smart and self-powered systems integrating energy harvesting, energy conversion, and energy storage are deemed as promising next-generation intelligent electronics. However, integration of multiple functions will create more challenges. It is suggested to evaluate the application scenario (working condition and device structure) prior to selection of electrode materials, electrolyte, and the integration process. SCs connected in series or in parallel can be the way to reach the energy and power requirement. The efficiency and durability of the integrated systems are also to be optimized. For example, in implantable applications, biodegradable materials are needed for the integration, while life-span of the integrated system should be long enough for well operation and short enough to allow bio-degradation.

With judicious selection of characterization methods discussed in this essay, mechanism understanding of SCs that are based on different electrode materials can be effectively achieved. Construction of multifunctional SCs with lightweight and high efficiency will also undoubtedly expand the application areas of SCs. A renaissance of electrochemical SCs is expected with deeper understanding of electrochemical mechanism on one hand, and realization of multifunctional SCs with lightweight and high efficiency on another.

Acknowledgements

The authors acknowledge the funding support by the National Research Foundation, Prime Minister's Office, Singapore, under its Campus for Research Excellence and Technological Enterprise (CREATE) program.

Conflict of Interest

The authors declare no conflict of interest.

Keywords

electrochemical supercapacitors, mechanistic understanding, multifunctional applications

Received: October 20, 2020
Revised: November 21, 2020
Published online: December 21, 2020

[1] a) N. Choudhary, C. Li, J. Moore, N. Nagaiah, L. Zhai, Y. Jung, J. Thomas, *Adv. Mater.* **2017**, *29*, 1605336; b) W. Raza, F. Ali, N. Raza, Y. Luo, K.-H. Kim, J. Yang, S. Kumar, A. Mehmood, E. E. Kwon, *Nano Energy* **2018**, *52*, 441.
[2] J. Yan, S. Li, B. Lan, Y. Wu, P. S. Lee, *Adv. Funct. Mater.* **2019**, *30*, 1902564.
[3] J. Chen, X. Wang, J. Wang, P. S. Lee, *Adv. Energy Mater.* **2016**, *6*, 1501745.
[4] A. Borenstein, O. Hanna, R. Attias, S. Luski, T. Brousse, D. Aurbach, *J. Mater. Chem. A* **2017**, *5*, 12653.
[5] Q. Meng, K. Cai, Y. Chen, L. Chen, *Nano Energy* **2017**, *36*, 268.
[6] Z. Lin, P. Rozier, B. Duployer, P.-L. Taberna, B. Anasori, Y. Gogotsi, P. Simon, *Electrochem. Commun.* **2016**, *72*, 50.
[7] C. Tanggarnjanavalukul, N. Phattharasupakun, J. Wutthiprom, P. Kidkhunthod, M. Sawangphruk, *Electrochim. Acta* **2018**, *273*, 17.
[8] A. C. Forse, J. M. Griffin, C. Merlet, J. Carretero-Gonzalez, A.-R. O. Raji, N. M. Trease, C. P. Grey, *Nat. Energy* **2017**, *2*, 16216.
[9] X. Tao, J. Du, Y. Sun, S. Zhou, Y. Xia, H. Huang, Y. Gan, W. Zhang, X. Li, *Adv. Funct. Mater.* **2013**, *23*, 4745.
[10] R. Futamura, T. Iiyama, Y. Takasaki, Y. Gogotsi, M. J. Biggs, M. Salanne, J. Segalini, P. Simon, K. Kaneko, *Nat. Mater.* **2017**, *16*, 1225.
[11] J. M. Black, G. Feng, P. F. Fulvio, P. C. Hillesheim, S. Dai, Y. Gogotsi, P. T. Cummings, S. V. Kalinin, N. Balke, *Adv. Energy Mater.* **2014**, *4*, 1300683.
[12] D. Chen, D. Ding, X. Li, G. H. Waller, X. Xiong, M. A. El-Sayed, M. Liu, *Chem. Mater.* **2015**, *27*, 6608.
[13] A. Sumboja, U. M. Tefashe, G. Wittstock, P. S. Lee, *Adv. Mater. Interfaces* **2015**, *2*, 1400154.
[14] M. D. Levi, L. Daikhin, D. Aurbach, V. Presser, *Electrochem. Commun.* **2016**, *67*, 16.
[15] H.-P. Cong, X.-C. Ren, P. Wang, S.-H. Yu, *Energy Environ. Sci.* **2013**, *6*, 1185.
[16] Y. Huang, M. Zhong, Y. Huang, M. Zhu, Z. Pei, Z. Wang, Q. Xue, X. Xie, C. Zhi, *Nat. Commun.* **2015**, *6*, 10310.
[17] P. Yang, P. Sun, W. Mai, *Mater. Today* **2016**, *19*, 394.
[18] Z. Zhang, X. Chen, P. Chen, G. Guan, L. Qiu, H. Lin, Z. Yang, W. Bai, Y. Luo, H. Peng, *Adv. Mater.* **2014**, *26*, 466.
[19] D. Pang, M. Alhabeb, X. Mu, Y. Dall'Agnese, Y. Gogotsi, Y. Gao, *Nano Lett.* **2019**, *19*, 7443.
[20] C. Chen, J. Cao, Q. Lu, X. Wang, L. Song, Z. Niu, J. Chen, *Adv. Funct. Mater.* **2017**, *27*, 1604639.
[21] J. Chen, D. H. Chua, P. S. Lee, *Small Methods* **2020**, *4*, 1900648.
[22] O. Ghodbane, F. Ataherian, N.-L. Wu, F. Favier, *J. Power Sources* **2012**, *206*, 454.
[23] C. Prehal, C. Koczwara, N. Jäckel, H. Amenitsch, V. Presser, O. Paris, *Phys. Chem. Chem. Phys.* **2017**, *19*, 15549.
[24] M. D. Levi, M. R. Lukatskaya, S. Sigalov, M. Beidaghi, N. Shpigel, L. Daikhin, D. Aurbach, M. W. Barsoum, Y. Gogotsi, *Adv. Energy Mater.* **2015**, *5*, 1400815.
[25] D. Chen, X. Xiong, B. Zhao, M. A. Mahmoud, M. A. El-Sayed, M. Liu, *Adv. Sci.* **2016**, *3*, 1500433.
[26] H.-W. Chang, Y.-R. Lu, J.-L. Chen, C.-L. Chen, J.-F. Lee, J.-M. Chen, Y.-C. Tsai, P.-H. Yeh, W. C. Chou, C.-L. Dong, *Phys. Chem. Chem. Phys.* **2016**, *18*, 18705.
[27] H. Wang, A. C. Forse, J. M. Griffin, N. M. Trease, L. Trognko, P.-L. Taberna, P. Simon, C. P. Grey, *J. Am. Chem. Soc.* **2013**, *135*, 18968.
[28] J. Come, V. Augustyn, J. W. Kim, P. Rozier, P.-L. Taberna, P. Gogotsi, J. W. Long, B. Dunn, P. Simon, *J. Electrochem. Soc.* **2014**, *161*, A718.
[29] M. R. Lukatskaya, O. Mashtalir, C. E. Ren, Y. Dall'Agnese, P. Rozier, P. L. Taberna, M. Naguib, P. Simon, M. W. Barsoum, Y. Gogotsi, *Science* **2013**, *341*, 1502.
[30] C. Koczwara, C. Prehal, S. Haas, P. Boesecke, N. Huesing, O. Paris, *ACS Appl. Mater. Interfaces* **2019**, *11*, 42214.

[31] C. Prehal, C. Koczwara, N. Jäckel, A. Schreiber, M. Burian, H. Amenitsch, M. A. Hartmann, V. Presser, O. Paris, *Nat. Energy* **2017**, *2*, 16215.
[32] N. Jäckel, S. Patrick Emge, B. Krüner, B. Roling, V. Presser, *J. Phys. Chem. C* **2017**, *121*, 19120.
[33] M. Hantel, V. Presser, R. Kötz, Y. Gogotsi, *Electrochem. Commun.* **2011**, *13*, 1221.
[34] N. Shpigel, M. D. Levi, S. Sigalov, L. Daikhin, D. Aurbach, *Acc. Chem. Res.* **2018**, *51*, 69.
[35] M. K. Dey, P. K. Sahoo, A. K. Satpati, *J. Electroanal. Chem.* **2017**, *788*, 175.
[36] J. Zhou, L. Hou, S. Luan, J. Zhu, H. Gou, D. Wang, F. Gao, *Small* **2018**, *14*, 1801897.
[37] N. Shpigel, M. D. Levi, S. Sigalov, O. Girshevitz, D. Aurbach, L. Daikhin, P. Pikma, M. Marandi, A. Janes, E. Lust, N. Jackel, V. Presser, *Nat. Mater.* **2016**, *15*, 570.
[38] J. L. S. Antonio, V. L. Martins, S. I. Córdoba de Torresi, R. M. Torresi, *Electrochim. Acta* **2019**, *324*, 134887.
[39] F. W. Richey, C. Tran, V. Kalra, Y. A. Elabd, *J. Phys. Chem. C* **2014**, *118*, 21846.
[40] M. Hu, Z. Li, T. Hu, S. Zhu, C. Zhang, X. Wang, *ACS Nano* **2016**, *10*, 11344.
[41] F. W. Richey, B. Dyatkin, Y. Gogotsi, Y. A. Elabd, *J. Am. Chem. Soc.* **2013**, *135*, 12818.
[42] Y. C. Chen, Y. G. Lin, Y. K. Hsu, S. C. Yen, K. H. Chen, L. C. Chen, *Small* **2014**, *10*, 3803.
[43] J. Chen, L. Mohrhusen, G. Ali, S. Li, K. Y. Chung, K. Al-Shamery, P. S. Lee, *Adv. Funct. Mater.* **2019**, *29*, 1807753.
[44] H.-W. Chang, Y.-R. Lu, J.-L. Chen, C.-L. Chen, J.-F. Lee, J.-M. Chen, Y.-C. Tsai, C.-M. Chang, P.-H. Yeh, W.-C. Chou, *Nanoscale* **2015**, *7*, 1725.
[45] M. P. Yeager, D. Su, N. S. Marinković, X. Teng, *J. Electrochem. Soc.* **2012**, *159*, A1598.
[46] P. Pande, A. Deb, A. E. Sleightholme, A. Djire, P. G. Rasmussen, J. Penner-Hahn, L. T. Thompson, *J. Power Sources* **2015**, *289*, 154.
[47] G. Oukali, E. Salager, M. R. Ammar, C.-E. Dutoit, V. Sarou-Kanian, P. Simon, E. Raymundo-Piñero, M. l. Deschamps, *ACS Nano* **2019**, *13*, 12810.
[48] Z.-X. Luo, Y.-Z. Xing, S. Liu, Y.-C. Ling, A. Kleinhammes, Y. Wu, *J. Phys. Chem. Lett.* **2015**, *6*, 5022.
[49] G. Wittstock, M. Burchardt, S. E. Pust, Y. Shen, C. Zhao, *Angew. Chem., Int. Ed.* **2007**, *46*, 1584.
[50] a) D. Polcari, P. Dauphin-Ducharme, J. Mauzeroll, *Chem. Rev.* **2016**, *116*, 13234; b) D. A. Walsh, K. R. Lovelock, P. Licence, *Chem. Soc. Rev.* **2010**, *39*, 4185.
[51] A. Sumboja, U. M. Tefashe, G. Wittstock, P. S. Lee, *J. Power Sources* **2012**, *207*, 205.
[52] J. Park, V. Kumar, X. Wang, P. S. Lee, W. Kim, *ACS Appl. Mater. Interfaces* **2017**, *9*, 33728.
[53] O. Munteshari, J. Lau, D. S. Ashby, B. Dunn, L. Pilon, *J. Electrochem. Soc.* **2018**, *165*, A1547.
[54] P. Suktha, P. Chiochan, A. Krittayavathananon, S. Sarawutanukul, S. Sethuraman, M. Sawangphruk, *RSC Adv.* **2019**, *9*, 28569.
[55] N. Batisse, E. n. Raymundo-Piñero, *ACS Appl. Mater. Interfaces* **2017**, *9*, 41224.
[56] X. Su, J. Ye, Y. Zhu, *J. Energy Chem.* **2021**, *54*, 242.
[57] Z. Lin, P.-L. Taberna, P. Simon, *Curr. Opin. Electrochem.* **2018**, *9*, 18.
[58] T. Wang, H. C. Chen, F. Yu, X. S. Zhao, H. Wang, *Energy Storage Mater.* **2019**, *16*, 545.
[59] X. Ma, W. Luo, M. Yan, L. He, L. Mai, *Nano Energy* **2016**, *24*, 165.
[60] Y. Ke, J. Chen, G. Lin, S. Wang, Y. Zhou, J. Yin, P. S. Lee, Y. Long, *Adv. Energy Mater.* **2019**, *9*, 1902066.
[61] F. Wang, X. Wu, X. Yuan, Z. Liu, Y. Zhang, L. Fu, Y. Zhu, Q. Zhou, Y. Wu, W. Huang, *Chem. Soc. Rev.* **2017**, *46*, 6816.
[62] P. Zhang, F. Wang, S. Yang, G. Wang, M. Yu, X. Feng, *Energy Storage Mater.* **2020**, *28*, 160.
[63] P. Zhang, F. Wang, M. Yu, X. Zhuang, X. Feng, *Chem. Soc. Rev.* **2018**, *47*, 7426.
[64] X. Zhao, B. Zheng, T. Huang, C. Gao, *Nanoscale* **2015**, *7*, 9399.
[65] Q. Wang, X. Wang, B. Liu, G. Yu, X. Hou, D. Chen, G. Shen, *J. Mater. Chem. A* **2013**, *1*, 2468.
[66] G. Xu, C. Zheng, Q. Zhang, J. Huang, M. Zhao, J. Nie, X. Wang, F. Wei, *Nano Res.* **2011**, *4*, 870.
[67] J. Ren, W. Bai, G. Guan, Y. Zhang, H. Peng, *Adv. Mater.* **2013**, *25*, 5965.
[68] S. Zhai, W. Jiang, L. Wei, H. E. Karahan, Y. Yuan, A. K. Ng, Y. Chen, *Mater. Horiz.* **2015**, *2*, 598.
[69] S.-L. Chou, J.-Z. Wang, S.-Y. Chew, H.-K. Liu, S.-X. Dou, *Electrochem. Commun.* **2008**, *10*, 1724.
[70] C. Meng, C. Liu, L. Chen, C. Hu, S. Fan, *Nano Lett.* **2010**, *10*, 4025.
[71] Y. Jin, H. Chen, M. Chen, N. Liu, Q. Li, *ACS Appl. Mater. Interfaces* **2013**, *5*, 3408.
[72] J. A. Lee, M. K. Shin, S. H. Kim, H. U. Cho, G. M. Spinks, G. G. Wallace, M. D. Lima, X. Lepró, M. E. Kozlov, R. H. Baughman, *Nat. Commun.* **2013**, *4*, 1970.
[73] W. Chen, R. Rakhi, L. Hu, X. Xie, Y. Cui, H. N. Alshareef, *Nano Lett.* **2011**, *11*, 5165.
[74] a) D. Ge, L. Yang, L. Fan, C. Zhang, X. Xiao, Y. Gogotsi, S. Yang, *Nano Energy* **2015**, *11*, 568.
[75] H. Sun, S. Xie, Y. Li, Y. Jiang, X. Sun, B. Wang, H. Peng, *Adv. Mater.* **2016**, *28*, 8431.
[76] a) P. Xu, T. Gu, Z. Cao, B. Wei, J. Yu, F. Li, J. H. Byun, W. Lu, Q. Li, T. W. Chou, *Adv. Energy Mater.* **2014**, *4*, 1300759; b) X. Chen, H. Lin, P. Chen, G. Guan, J. Deng, H. Peng, *Adv. Mater.* **2014**, *26*, 4444.
[77] Y. Xie, Y. Liu, Y. Zhao, Y. H. Tsang, S. P. Lau, H. Huang, Y. Chai, *J. Mater. Chem. A* **2014**, *2*, 9142.
[78] T. Chen, R. Hao, H. Peng, L. Dai, *Angew. Chem., Int. Ed.* **2015**, *54*, 618.
[79] Z. Yang, J. Deng, X. Chen, J. Ren, H. Peng, *Angew. Chem., Int. Ed.* **2013**, *52*, 13453.
[80] A. Lamberti, F. Clerici, M. Fontana, L. Scaltrito, *Adv. Energy Mater.* **2016**, *6*, 1600050.
[81] Z. Zhang, L. Wang, Y. Li, Y. Wang, J. Zhang, G. Guan, Z. Pan, G. Zheng, H. Peng, *Adv. Energy Mater.* **2017**, *7*, 1601814.
[82] S. Park, A. W. M. Tan, J. Wang, P. S. Lee, *Nanoscale Horiz.* **2017**, *2*, 199.
[83] Y. Huang, Y. Huang, M. Zhu, W. Meng, Z. Pei, C. Liu, H. Hu, C. Zhi, *ACS Nano* **2015**, *9*, 6242.
[84] Y. Huang, M. Zhu, Z. Pei, Q. Xue, Y. Huang, C. Zhi, *J. Mater. Chem. A* **2016**, *4*, 1290.
[85] W. Wang, J. Yan, J. Liu, D. Ou, Q. Qin, B. Lan, Y. Ning, D. Zhou, Y. Wu, *Electrochim. Acta* **2018**, *282*, 835.
[86] H. Wang, B. Zhu, W. Jiang, Y. Yang, W. R. Leow, H. Wang, X. Chen, *Adv. Mater.* **2014**, *26*, 3638.
[87] H. Sun, X. You, Y. Jiang, G. Guan, X. Fang, J. Deng, P. Chen, Y. Luo, H. Peng, *Angew. Chem., Int. Ed.* **2014**, *53*, 9526.
[88] P. Cordier, F. Tournilhac, C. Soulie-Ziakovic, L. Leibler, *Nature* **2008**, *451*, 977.
[89] S. Park, G. Thangavel, K. Parida, S. Li, P. S. Lee, *Adv. Mater.* **2019**, *31*, 1805536.
[90] Y. Li, S. Chen, M. Wu, J. Sun, *ACS Appl. Mater. Interfaces* **2014**, *6*, 16409.
[91] a) T. J. Trivedi, D. Bhattacharjya, J. S. Yu, A. Kumar, *ChemSusChem* **2015**, *8*, 3294; b) Y. Shi, Y. Zhang, L. Jia, Q. Zhang, X. Xu, *ACS Appl. Mater. Interfaces* **2018**, *10*, 36028; c) H. Liao, F. Zhou, Z. Zhang, J. Yang, *Chem. Eng. J.* **2019**, *357*, 428.
[92] Y. Guo, X. Zhou, Q. Tang, H. Bao, G. Wang, P. Saha, *J. Mater. Chem. A* **2016**, *4*, 8769.
[93] F. Tao, L. Qin, Z. Wang, Q. Pan, *ACS Appl. Mater. Interfaces* **2017**, *9*, 15541.

[94] L. Liu, B. Shen, D. Jiang, R. Guo, L. Kong, X. Yan, *Adv. Energy Mater.* **2016**, *6*, 1600763.
[95] J. Deng, Y. Zhang, Y. Zhao, P. Chen, X. Cheng, H. Peng, *Angew. Chem., Int. Ed.* **2015**, *54*, 15419.
[96] J. Zhong, J. Meng, Z. Yang, P. Poulin, N. Koratkar, *Nano Energy* **2015**, *17*, 330.
[97] a) R. Kötz, M. Hahn, R. Gallay, *J. Power Sources* **2006**, *154*, 550; b) A. Tatlisu, Z. Huang, R. Chen, *ChemSusChem* **2018**, *11*, 3899.
[98] X. Liu, P. G. Pickup, *Energy Environ. Sci.* **2008**, *1*, 494.
[99] Y. Yang, S. W. Ng, D. Chen, J. Chang, D. Wang, J. Shang, Q. Huang, Y. Deng, Z. Zheng, *Small* **2019**, *15*, e1902071.
[100] H. Yu, N. Rouelle, A. Qiu, J.-A. Oh, D. M. Kempaiah, J. D. Whittle, M. Aakyiir, W. Xing, J. Ma, *ACS Appl. Mater. Interfaces* **2020**, *12*, 37977.
[101] X. Li, L. Liu, X. Wang, Y. S. Ok, J. A. W. Elliott, S. X. Chang, H. J. Chung, *Sci. Rep.* **2017**, *7*, 1685.
[102] Q. Rong, W. Lei, J. Huang, M. Liu, *Adv. Energy Mater.* **2018**, *8*, 1801967.
[103] Q. Dou, S. Lei, D.-W. Wang, Q. Zhang, D. Xiao, H. Guo, A. Wang, H. Yang, Y. Li, S. Shi, X. Yan, *Energy Environ. Sci.* **2018**, *11*, 3212.
[104] Y. Sun, Y. Wang, L. Liu, B. Liu, Q. Zhang, D. Wu, H. Zhang, X. Yan, *J. Mater. Chem. A* **2020**, *8*, 17998.
[105] J. Lang, X. Zhang, L. Liu, B. Yang, J. Yang, X. Yan, *J. Power Sources* **2019**, *423*, 271.
[106] J. Xu, N. Yuan, J. M. Razal, Y. Zheng, X. Zhou, J. Ding, K. Cho, S. Ge, R. Zhang, Y. Gogotsi, R. H. Baughman, *Energy Storage Mater.* **2019**, *22*, 323.
[107] J. Xu, X. Wang, X. Zhou, N. Yuan, S. Ge, J. Ding, *Electrochim. Acta* **2019**, *301*, 478.
[108] X. Wang, B. Liu, Q. Wang, W. Song, X. Hou, D. Chen, Y.-b. Cheng, G. Shen, *Adv. Mater.* **2013**, *25*, 1479.
[109] J. Yun, Y. Lim, H. Lee, G. Lee, H. Park, S. Y. Hong, S. W. Jin, Y. H. Lee, S.-S. Lee, J. S. Ha, *Adv. Funct. Mater.* **2017**, *27*, 1700135.
[110] X. Dong, Y. Cao, J. Wang, M. B. Chan-Park, L. Wang, W. Huang, P. Chen, *RSC Adv.* **2012**, *2*, 4364.
[111] Y. Liu, Y. Jiao, Z. Zhang, F. Qu, A. Umar, X. Wu, *ACS Appl. Mater. Interfaces* **2014**, *6*, 2174.
[112] Y. Huang, S. V. Kershaw, Z. Wang, Z. Pei, J. Liu, Y. Huang, H. Li, M. Zhu, A. L. Rogach, C. Zhi, *Small* **2016**, *12*, 3393.
[113] Y. Song, H. Chen, Z. Su, X. Chen, L. Miao, J. Zhang, X. Cheng, H. Zhang, *Small* **2017**, *13*, 1702091.
[114] J. Zhao, Y. Zhang, Y. Huang, J. Xie, X. Zhao, C. Li, J. Qu, Q. Zhang, J. Sun, B. He, Q. Li, C. Lu, X. Xu, W. Lu, L. Li, Y. Yao, *Adv. Sci.* **2018**, *5*, 1801114.
[115] X. Wang, B. Liu, R. Liu, Q. Wang, X. Hou, D. Chen, R. Wang, G. Shen, *Angew. Chem., Int. Ed.* **2014**, *53*, 1849.
[116] F. S. Omar, A. Numan, N. Duraisamy, S. Bashir, K. Ramesh, S. Ramesh, *J. Alloys Compd.* **2017**, *716*, 96.
[117] J. Yun, Y. Lim, G. N. Jang, D. Kim, S.-J. Lee, H. Park, S. Y. Hong, G. Lee, G. Zi, J. S. Ha, *Nano Energy* **2016**, *19*, 401.
[118] M. Weng, Y. Duan, P. Zhou, F. Huang, W. Zhang, L. Chen, *Nano Energy* **2020**, *68*, 104365.
[119] J. Torop, V. Palmre, M. Arulepp, T. Sugino, K. Asaka, A. Aabloo, *Carbon* **2011**, *49*, 3113.
[120] J. Liang, Y. Huang, J. Oh, M. Kozlov, D. Sui, S. Fang, R. H. Baughman, Y. Ma, Y. Chen, *Adv. Funct. Mater.* **2011**, *21*, 3778.
[121] P. Yang, P. Sun, Z. Chai, L. Huang, X. Cai, S. Tan, J. Song, W. Mai, *Angew. Chem., Int. Ed.* **2014**, *53*, 11935.
[122] S. Cong, Y. Tian, Q. Li, Z. Zhao, F. Geng, *Adv. Mater.* **2014**, *26*, 4260.
[123] G. Cai, X. Wang, M. Cui, P. Darmawan, J. Wang, A. L.-S. Eh, P. S. Lee, *Nano Energy* **2015**, *12*, 258.
[124] H. S. Chavan, B. Hou, A. T. A. Ahmed, Y. Jo, S. Cho, J. Kim, S. M. Pawar, S. Cha, A. I. Inamdar, H. Im, H. Kim, *Sol. Energy Mater. Sol. Cells* **2018**, *185*, 166.
[125] D. Wei, M. R. J. Scherer, C. Bower, P. Andrew, T. Ryhänen, U. Steiner, *Nano Lett.* **2012**, *12*, 1857.
[126] R. Yuksel, S. C. Cevher, A. Cirpan, L. Toppare, H. E. Unalan, *J. Electrochem. Soc.* **2015**, *162*, A2805.
[127] G. Cai, P. Darmawan, M. Cui, J. Wang, J. Chen, S. Magdassi, P. S. Lee, *Adv. Energy Mater.* **2016**, *6*, 1501882.
[128] R. T. Ginting, M. M. Ovhal, J.-W. Kang, *Nano Energy* **2018**, *53*, 650.
[129] K. Wang, H. Wu, Y. Meng, Y. Zhang, Z. Wei, *Energy Environ. Sci.* **2012**, *5*, 8384.
[130] T. An, Y. Ling, S. Gong, B. Zhu, Y. Zhao, D. Dong, L. W. Yap, Y. Wang, W. Cheng, *Adv. Mater. Technol.* **2019**, *4*, 1800473.
[131] K. Zhou, H. Wang, J. Jiu, J. Liu, H. Yan, K. Suganuma, *Chem. Eng. J.* **2018**, *345*, 290.
[132] G. Cai, J. Chen, J. Xiong, A. Lee-Sie Eh, J. Wang, M. Higuchi, P. S. Lee, *ACS Energy Lett.* **2020**, *5*, 1159.
[133] X. Chen, H. Lin, J. Deng, Y. Zhang, X. Sun, P. Chen, X. Fang, Z. Zhang, G. Guan, H. Peng, *Adv. Mater.* **2014**, *26*, 8126.
[134] T. G. Yun, M. Park, D. H. Kim, D. Kim, J. Y. Cheong, J. G. Bae, S. M. Han, I. D. Kim, *ACS Nano* **2019**, *13*, 3141.
[135] P. Du, X. Hu, C. Yi, H. C. Liu, P. Liu, H.-L. Zhang, X. Gong, *Adv. Funct. Mater.* **2015**, *25*, 2420.
[136] X. Xu, S. Li, H. Zhang, Y. Shen, S. M. Zakeeruddin, M. Graetzel, Y.-B. Cheng, M. Wang, *ACS Nano* **2015**, *9*, 1782.
[137] R. Liu, J. Wang, T. Sun, M. Wang, C. Wu, H. Zou, T. Song, X. Zhang, S.-T. Lee, Z. L. Wang, *Nano Lett.* **2017**, *17*, 4240.
[138] J. Xu, Z. Ku, Y. Zhang, D. Chao, H. J. Fan, *Adv. Mater. Technol.* **2016**, *1*, 1600074.
[139] H. Sun, X. You, J. Deng, X. Chen, Z. Yang, P. Chen, X. Fang, H. Peng, *Angew. Chem., Int. Ed.* **2014**, *53*, 6664.
[140] F. Wang, C. Jiang, C. Tang, S. Bi, Q. Wang, D. Du, J. Song, *Nano Energy* **2016**, *21*, 209.
[141] A. Ramadoss, B. Saravanakumar, S. W. Lee, Y.-S. Kim, S. J. Kim, Z. L. Wang, *ACS Nano* **2015**, *9*, 4337.
[142] K. Parida, V. Bhavanasi, V. Kumar, J. Wang, P. S. Lee, *J. Power Sources* **2017**, *342*, 70.
[143] P. Pazhamalai, K. Krishnamoorthy, V. K. Mariappan, S. Sahoo, S. Manoharan, S.-J. Kim, *Adv. Mater. Interfaces* **2018**, *5*, 1800055.
[144] A. Maitra, S. K. Karan, S. Paria, A. K. Das, R. Bera, L. Halder, S. K. Si, A. Bera, B. B. Khatua, *Nano Energy* **2017**, *40*, 633.
[145] J. Luo, F. R. Fan, T. Jiang, Z. Wang, W. Tang, C. Zhang, M. Liu, G. Cao, Z. L. Wang, *Nano Res.* **2015**, *8*, 3934.
[146] Q. Jiang, C. Wu, Z. Wang, A. C. Wang, J.-H. He, Z. L. Wang, H. N. Alshareef, *Nano Energy* **2018**, *45*, 266.
[147] J. Wang, Z. Wen, Y. Zi, P. Zhou, J. Lin, H. Guo, Y. Xu, Z. L. Wang, *Adv. Funct. Mater.* **2016**, *26*, 1070.
[148] J. Wang, X. Li, Y. Zi, S. Wang, Z. Li, L. Zheng, F. Yi, S. Li, Z. L. Wang, *Adv. Mater.* **2015**, *27*, 4830.
[149] H. Guo, M.-H. Yeh, Y. Zi, Z. Wen, J. Chen, G. Liu, C. Hu, Z. L. Wang, *ACS Nano* **2017**, *11*, 4475.
[150] X. Pu, L. Li, M. Liu, C. Jiang, C. Du, Z. Zhao, W. Hu, Z. L. Wang, *Adv. Mater.* **2016**, *28*, 98.
[151] K. Dong, Y. C. Wang, J. Deng, Y. Dai, S. L. Zhang, H. Zou, B. Gu, B. Sun, Z. L. Wang, *ACS Nano* **2017**, *11*, 9490.
[152] H. Wang, D. Zhao, Z. U. Khan, S. Puzinas, M. P. Jonsson, M. Berggren, X. Crispin, *Adv. Electron. Mater.* **2017**, *3*, 1700013.
[153] M. Bonetti, S. Nakamae, M. Roger, P. Guenoun, *J. Chem. Phys.* **2011**, *134*, 114513.
[154] K. Yang, K. Cho, S. Yang, Y. Park, S. Kim, *Nano Energy* **2019**, *60*, 667.
[155] D. Zhao, H. Wang, Z. U. Khan, J. C. Chen, R. Gabrielsson, M. P. Jonsson, M. Berggren, X. Crispin, *Energy Environ. Sci.* **2016**, *9*, 1450.

[156] J. Wang, S. P. Feng, Y. Yang, N. Y. Hau, M. Munro, E. Ferreira-Yang, G. Chen, *Nano Lett.* **2015**, *15*, 5784.
[157] S. Jung, J. Lee, T. Hyeon, M. Lee, D.-H. Kim, *Adv. Mater.* **2014**, *26*, 6329.
[158] J. Zou, M. Zhang, J. Huang, J. Bian, Y. Jie, M. Willander, X. Cao, N. Wang, Z. L. Wang, *Adv. Energy Mater.* **2018**, *8*, 1702671.
[159] N. Wang, W. Dou, S. Hao, Y. Cheng, D. Zhou, X. Huang, C. Jiang, X. Cao, *Nano Energy* **2019**, *56*, 868.
[160] Z. Wen, M.-H. Yeh, H. Guo, J. Wang, Y. Zi, W. Xu, J. Deng, L. Zhu, X. Wang, C. Hu, *Sci. Adv.* **2016**, *2*, e1600097.
[161] a) K. Liu, C. Yu, W. Guo, L. Ni, J. Yu, Y. Xie, Z. Wang, Y. Ren, J. Qiu, *J. Energy Chem.* **2020**, https://doi.org/10.1016/j.jechem.2020.09.041; b) Z. Wang, X. Chu, Z. Xu, H. Su, C. Yan, F. Liu, B. Gu, H. Huang, D. Xiong, H. Zhang, W. Deng, H. Zhang, W. Yang, *J. Mater. Chem. A* **2019**, *7*, 8633.
[162] Z. Wang, Z. Xu, H. Huang, X. Chu, Y. Xie, D. Xiong, C. Yan, H. Zhao, H. Zhang, W. Yang, *ACS Nano* **2020**, *14*, 4916.
[163] Z. Huang, A. Chen, F. Mo, G. Liang, X. Li, Q. Yang, Y. Guo, Z. Chen, Q. Li, B. Dong, C. Zhi, *Adv. Energy Mater.* **2020**, *10*, 2001024.

Pooi See Lee is a full professor at the School of Materials Science and Engineering, Nanyang Technological University (NTU), Singapore. She obtained her B.Sc. (Hons.) and Ph.D. at the National University of Singapore. Her research work focuses on the theme of electrochemical- and electrical-inspired devices based on nanostructures and nanocomposites, and human machine interface. Her works have demonstrated applications in electrochromics, energy storages, stretchable devices, electrical memory devices, light emission devices, nanowire transistors, photodetectors, and sensors. She currently serves as the Dean of the Graduate College, NTU.

